# OPTICAL STOCHASTIC COOLING

V. Lebedev[1], Fermilab, Batavia, IL 60510, U.S.A.

*Abstract*

Intrabeam scattering and other diffusion mechanisms result in a growth of beam emittances and luminosity degradation in hadron colliders. In particular, at the end of Tevatron Run II when optimal collider operation was achieved only about 40% of antiprotons were burned in collisions to the store end and the rest were discarded. Taking into account a limited rate of antiproton production further growth of the integral luminosity was not possible without beam cooling. Similar problems limit the integral luminosity in the RHIC operating with protons. For both cases beam cooling is the only effective remedy to increase the luminosity integral. Unfortunately neither electron nor stochastic cooling can be effective at the beam energy and the bunch density required for modern hadron colliders. Even in the case of LHC where synchrotron radiation damping is already helpful for beam cooling its cooling rates are still insufficient to support an optimal operation of the collider. In this paper we consider principles and main limitations for the optical stochastic cooling (OSC) representing a promising technology capable to achieve required cooling rates. The OSC is based on the same principles as the normal microwave stochastic cooling but uses much smaller wave length resulting in a possibility of dense beam cooling.

## Introduction

The stochastic cooling was suggested by Simon Van der Meer [1]. It was critically important technology for success of the first proton-antiproton collider [2]. Since then it has been successfully used in a number of machines for particle cooling and accumulation. There is considerable literature on the subject. Here we would like to point out two references [3,4] reviewing its theory and development for the Tevatron Run II, as well as practical aspects of stochastic cooling usage. These papers also present extended bibliography on the subject.

Although the usage of stochastic cooling has been indispensable for antiproton accumulation and precooling its use is limited for bunched beam cooling at high energy. The bunched beam cooling has been demonstrated for heavy ions in RHIC [5] where the number of particles in the bunch is comparatively small. However it cannot be used for cooling of dense bunched beams in proton-(anti)proton colliders due to much larger number of particles per bunch and, consequently, much higher beam brightness. In the case of optimal cooling the maximum damping rate can be estimated as:

$$\frac{1}{\tau} \approx \frac{2W\sigma_s}{NC} \ , \qquad (1)$$

[1] val@fnal.gov

where $W$ is the bandwidth of the system, $N$ is the number of particles in the bunch, $\sigma_s$ is the rms bunch length, and $C$ is the machine circumference. Assuming a system with one octave band and upper boundary of 8 GHz one obtains $\tau = 12000$ hour for the LHC proton beam ($\sigma_s = 9$ cm, $C = 26.66$ km). Effective cooling requires damping rates being at least 3 orders of magnitude higher.

The OSC suggested in Ref. [6] was aimed to address this deficiency. Instead of microwave frequencies it operates at the optical frequencies and, consequently, it can have a bandwidth of $\sim 10^{14}$ Hz; thus, suggesting a way to achieve the required damping rates. The basic principles of the OSC are similar to the normal (microwave) stochastic cooling. The key difference is the use of optical frequencies, which allows one an increase of system bandwidth by almost 4 orders of magnitude.

Although the OSC was proposed 20 years ago it still was not tested in experiment. There were suggestions of its experimental implementation in Tevatron [7, 8], RHIC [9] but it was too risky to implement it on the operating collider and the work did not proceed beyond initial proposal. The first attempt to make a test of the OSC with small energy electrons was done in the BATES [10] but it did not get enough support. Presently, Fermilab is constructing a new ring [11,12] devoted to test of the integrable optics and the OSC.

In this paper we consider the theory of stochastic cooling and its implications to the beam and light optics.

## 1. Principle of OSC Operation

The wavelength of e.-m. radiation used in the OSC is orders of magnitude smaller than the transverse size of vacuum chamber. In this case usual pickups and kickers employed in the microwave stochastic cooling cannot be used; instead, undulators were suggested [6] to be used for both a pickup and a kicker. In other words, in the OSC a particle emits e.-m. radiation in the first (pickup) undulator. Then, the radiation amplified in an optical amplifier (OA) makes a longitudinal kick to the particle in the second (kicker) undulator as shown in Figure 1. Further we will call these undulators as the pickup and the kicker. Note that efficiency of transverse kicks is much smaller and therefore the OSC is based on the longitudinal kicks only. Cooling in other planes is based on the plane-to-plane coupling of particle motion. A magnetic chicane is used to make space for an OA and to bring the particle and its amplified radiation together in the kicker undulator.

In further consideration we assume that the path lengths of particle and radiation are adjusted so that the relative longitudinal momentum change of a particle is equal to:

$$\frac{\delta p}{p} = \kappa \sin(k\, s)\ . \tag{2}$$

Here $k = 2\pi/\lambda$ is the radiation wave number, and $s$ is the particle displacement on the way from pickup to kicker relative to the reference particle which obtains zero kick. In the linear approximation one can write:

$$s = M_{51}x + M_{52}\theta_x + M_{56}\left(\Delta p / p\right) , \tag{3}$$

where $M_{5n}$ are the elements of 6x6 transfer matrix from pickup to kicker, $x$, $\theta_x$ and $\Delta p/p$ are the particle coordinate, angle and relative momentum deviation in the pickup center. In such arrangement the horizontal cooling is achieved by coupling between horizontal and longitudinal motion in the chicane. The vertical cooling is supported by $x$-$y$ coupling in the rest of the ring.

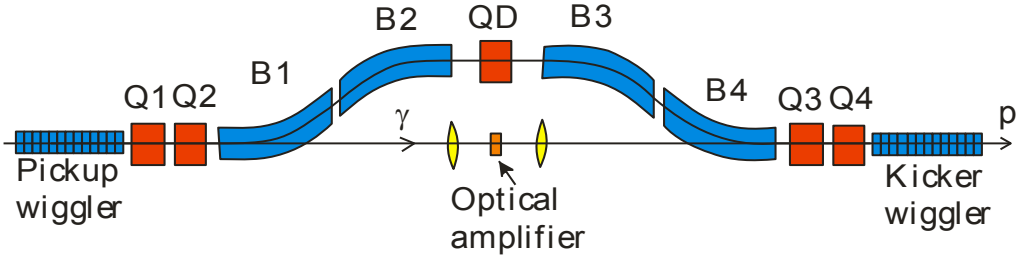


Figure 1: Layout of the cooling system.

## 2. Transfer Matrix for Coupled Longitudinal and Horizontal Motions

We assume that a particle motion in the cooling chicane is only coupled between longitudinal and horizontal planes. Consequently, the vertical motion is uncoupled and can be safely omitted from the below analysis. The motion symplecticity binds up the transfer matrix elements so that for 4x4 matrix only 10 of its 16 elements are independent. In the absence of longitudinal kicks between points 1 and 2 (see Figure 2) the matrix between them can be expressed through the Twiss parameters of the points and the $M_{56}$ element, so that:

$$\mathbf{M} = \begin{bmatrix} M_{11} & M_{12} & 0 & M_{16} \\ M_{21} & M_{22} & 0 & M_{26} \\ M_{51} & M_{52} & 1 & M_{56} \\ 0 & 0 & 0 & 1 \end{bmatrix}, \quad \mathbf{x} = \begin{bmatrix} x \\ \theta_x \\ s \\ \Delta p / p \end{bmatrix}. \tag{4}$$

Here the matrix elements of horizontal motion are well-known:

$$\begin{aligned} M_{11} &= \sqrt{\frac{\beta_2}{\beta_1}}\left(\cos\mu + \alpha_1 \sin\mu\right), & M_{12} &= \sqrt{\beta_1\beta_2}\,\sin\mu , \\ M_{21} &= \frac{\alpha_1 - \alpha_2}{\sqrt{\beta_1\beta_2}}\cos\mu - \frac{1+\alpha_1\alpha_2}{\sqrt{\beta_1\beta_2}}\sin\mu , & M_{22} &= \sqrt{\frac{\beta_1}{\beta_2}}\left(\cos\mu - \alpha_2 \sin\mu\right), \end{aligned} \tag{5}$$

and the matrix elements describing $x$-$s$ coupling are bound up by motion symplecticity,

$$\mathbf{M}^T\mathbf{U}\mathbf{M} = \mathbf{U} , \tag{6}$$

resulting:

$$\begin{aligned} M_{16} &= D_2 - M_{11}D_1 - M_{12}D_1' , \\ M_{26} &= D_2' - M_{21}D_1 - M_{22}D_1' , \\ M_{51} &= M_{21}M_{16} - M_{11}M_{26} , \\ M_{52} &= M_{22}M_{16} - M_{12}M_{26} , \end{aligned} \tag{7}$$

where $\beta_{1,2}$ and $\alpha_{1,2}$ are the beta-functions and their negative half derivatives at the points 1 and 2, $D_{1,2}$ and $D'_{1,2}$ are the dispersions and their derivatives, $\mu$ is the betatron phase advance between points 1 and 2, and

$$\mathbf{U} = \begin{bmatrix} 0 & 1 & 0 & 0 \\ -1 & 0 & 0 & 0 \\ 0 & 0 & 0 & 1 \\ 0 & 0 & -1 & 0 \end{bmatrix} \tag{8}$$

is the unit symplectic matrix. The matrix elements are enumerated similar to a 6x6 matrix but the elements related to the vertical motion (decoupled from other two degrees of freedom) are omitted. Note also that the symplecticity condition implies that the $s$ coordinate used in Eq. (2) and (4) represents particle displacement in the bunch frame but not the orbit lengthening often used in the definition of the transfer matrix, so that $\Delta L = \tilde{M}_{56}\Delta p / p$. For an ultra-relativistic bunch these two definitions are bound up as following:

$$M_{56} = \frac{1}{\gamma^2} - \tilde{M}_{56} \ . \tag{9}$$

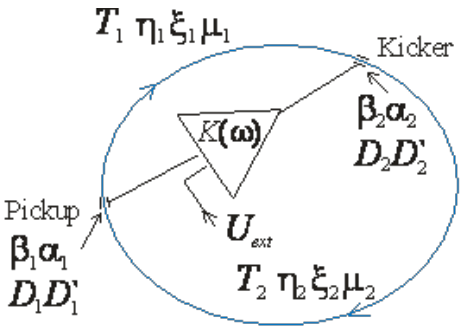


Figure 2: OSC schematic.

Similar to the ring slip-factor, $\eta = 1/\gamma^2 - \alpha$, we introduce the partial pickup-to-kicker slip-factor, $\eta_{12}$, which describes the longitudinal displacement for a particle with momentum deviation $\Delta p/p$ in the absence of betatron oscillations:

$$\eta_{12} = \frac{M_{51}D_1 + M_{52}D'_1 + M_{56}}{2\pi R} \ . \tag{10}$$

Here $\alpha$ is the ring momentum compaction, and $R$ is the average ring radius ($C = 2\pi R$). To simplify further formulas we also introduce the pickup-to-kicker slip-parameter $S_{12} = 2\pi R\eta_{12}$. Substituting the matrix elements from Eq. (7) one obtains:

$$S_{12} \equiv 2\pi R\eta_{12} = M_{56} - D_1 D_2 \left( \frac{1+\alpha_1\alpha_2}{\sqrt{\beta_1\beta_2}} \sin\mu_1 + \frac{\alpha_2-\alpha_1}{\sqrt{\beta_1\beta_2}} \cos\mu_1 \right) - D_1 D_2' \sqrt{\frac{\beta_2}{\beta_1}} \left(\cos\mu_1 + \alpha_1 \sin\mu_1\right)$$
$$+ D_1' D_2 \sqrt{\frac{\beta_1}{\beta_2}} \left(\cos\mu_1 - \alpha_2 \sin\mu_1\right) - D_1' D_2' \sqrt{\beta_1\beta_2} \sin\mu_1 \,, \tag{11}$$

where indices 1 and 2 mark the Twiss parameters at the pickup and kicker locations, correspondingly, and $\mu_1$ is the pickup-to-kicker betatron phase advance.

## 3. Ratio of Damping Rates

The longitudinal kick to a particle due to its interaction with own amplified radiation in the kicker is determined by Eq. (2). Leaving only linear term in the expansion of sin(*ks*) and expressing *s* through the particle positions in the pickup (see. Eq. (3)) one obtains:

$$\frac{\delta p}{p} = \kappa k \left( M_{1_{51}} x_1 + M_{1_{52}} \theta_{x_1} + M_{1_{56}} \frac{\Delta p}{p} \right) , \tag{12}$$

or in the matrix form:

$$\boldsymbol{\delta}\mathbf{x}_2 = \mathbf{M}_c \mathbf{x}_1 \,, \quad \mathbf{M}_c = k\kappa \begin{bmatrix} 0 & 0 & 0 & 0 \\ 0 & 0 & 0 & 0 \\ 0 & 0 & 0 & 0 \\ M_{1_{51}} & M_{1_{52}} & 0 & M_{1_{56}} \end{bmatrix} . \tag{13}$$

Here $\mathbf{x}_1$ is the vector of particle coordinates in the pickup, and we additionally denote the matrix elements of the pick-up to kicker transfer matrix by index 1. Taking this into account one can write down a kicker-to-kicker one turn map:

$$\left(\mathbf{x}_2\right)_{n+1} = \mathbf{M}_1 \mathbf{M}_2 \left(\mathbf{x}_2\right)_n + \left(\boldsymbol{\delta}\mathbf{x}_2\right)_n = \left(\mathbf{M}_0 + \mathbf{M}_c \mathbf{M}_2\right)\left(\mathbf{x}_2\right)_n \,, \tag{14}$$

where *n* enumerates turns, $\mathbf{M}_2$ is the kicker-to-pickup transfer matrix, $\mathbf{M}_0 = \mathbf{M}_1\,\mathbf{M}_2$ is the entire ring transfer matrix, $(\mathbf{x}_2)_n$ is related to the particle coordinates at *n*-th turn at the point immediately downstream of the kicker, and we took into account $\left(\mathbf{x}_1\right)_n = \mathbf{M}_2 \left(\mathbf{x}_2\right)_n$ .

The perturbation theory developed in Ref. [13] (see also [4] for details) for the case of symplectic unperturbed motion yields that the tune shifts are:

$$\delta Q_k = \frac{1}{4\pi} \mathbf{v}_k{}^{+} \mathbf{U}\, \mathbf{M}_c\, \mathbf{U} \mathbf{M}_1{}^{T} \mathbf{U}\, \mathbf{v}_k \,, \tag{15}$$

where $\mathbf{v}_k$ are two of four eigen-vectors of unperturbed motion chosen out of each complex conjugate pair and normalized so that $\mathbf{v}_k{}^{+} \mathbf{U}\, \mathbf{v}_k = -2i$ (k = 1,2). Performing matrix multiplication and taking into account that the symplecticity binds up $M_{51}$, $M_{52}$ and $M_{16}$, $M_{26}$ one finally obtains:

$$\delta Q_k = \frac{k\kappa}{4\pi}\mathbf{v}_k^{+}\begin{bmatrix} 0 & 0 & 0 & 0 \\ 0 & 0 & 0 & 0 \\ M_{1_{26}} & -M_{1_{16}} & 0 & M_{1_{56}} \\ 0 & 0 & 0 & 0 \end{bmatrix}\mathbf{v}_k \ . \tag{16}$$

In the case of small synchrotron tune, $\nu_s << 1$, one can neglect the effect of RF cavities on components of the eigen-vector related to the horizontal betatron motion. Then, the eigen-vector is equal to:

$$\mathbf{v}_1 = \begin{bmatrix} \sqrt{\beta_2} \\ -\left(i+\alpha_2\right)/\sqrt{\beta_2} \\ -\left(iD_2\left(1-i\alpha_2\right)+D_2'\beta_2\right)/\sqrt{\beta_2} \\ 0 \end{bmatrix} \ , \tag{17}$$

Substituting Eq. (17) to Eq. (16) and using Eq. (11) one obtains the damping rate (amplitude, per turn) of the betatron motion:

$$\lambda_1 \equiv \lambda_x = -2\pi \,\mathrm{Im}\,\delta Q_1 = -\frac{k\kappa}{2}\left(D_2 M_{1_{2,6}} - D_2' M_{1_{1,6}}\right) = -\frac{k\kappa}{2}\left(M_{1_{56}} - S_{12}\right) \ . \tag{18}$$

The condition $\nu_s << 1$ also allows one to neglect the betatron motion on the synchrotron motion. Consequently, for the second eigen-vector (related to the synchrotron motion) one obtains:

$$\mathbf{v}_2 = \begin{bmatrix} -iD_2/\sqrt{\beta_s} \\ -iD_2'/\sqrt{\beta_s} \\ \sqrt{\beta_s} \\ -i/\sqrt{\beta_s} \end{bmatrix} , \tag{19}$$

where $\beta_s = R\eta/\nu_s$ is the $\beta$-function of the longitudinal motion introduced so that $s_{\max} = \beta_s \left(\Delta p/p\right)_{\max}$. That yields the damping rate (amplitude, per turn) of the synchrotron motion:

$$\lambda_2 \equiv \lambda_s = -2\pi \,\mathrm{Im}\,\delta Q_2 = -\frac{k\kappa S_{12}}{2} \ . \tag{20}$$

Summing Eqs. (18) and (20) one obtains the sum of the damping rates:

$$\lambda_1 + \lambda_2 = -\frac{k\kappa}{2} M_{1_{56}} \ . \tag{21}$$

Although $M_{1_{56}}$ and, consequently, the sum of damping rates depend only on focusing inside the chicane, the ratio of damping rates depends on the dispersion at the chicane beginning, *i.e.* on the ring dispersion. Eqs. (18) and (20) yield the ratio of damping rates,

$$\frac{\lambda_x}{\lambda_s} = \frac{M_{l_{56}}}{S_{12}} - 1 \ . \tag{22}$$

## 4. The Cooling Range

The cooling force is linear for small amplitude oscillations only. Combining Eqs. (2) and (3), and performing simple transformations one obtains:

$$\frac{\delta p}{p} = \kappa \sin\left(a_x \sin(\psi_x) + a_p \sin(\psi_p)\right) \ , \tag{23}$$

where $a_x$, $a_p$, $\psi_x$ and $\psi_p$ are the dimensionless amplitudes (expressed in the phase advance of laser wave) and phases of pickup-to-kicker path lengthening due to betatron and synchrotron motions. The dimensionless amplitude due to synchrotron motion directly follows from Eq. (10):

$$a_p = k\left(M_{l_{51}} D_1 + M_{l_{52}} D_1' + M_{l_{56}}\right)\left(\frac{\Delta p}{p}\right)_m \ , \tag{24}$$

where $(\Delta p/p)_m$ is the amplitude of momentum oscillations. To find the dimensionless amplitude due to betatron motion we express particle coordinates through its Courant-Snyder invariant[2], $\tilde{\varepsilon}$ , and phase, $\psi$:

$$\begin{aligned} x_1 &= \sqrt{\tilde{\varepsilon}\beta_1}\cos\psi \ , \\ \theta_{x_1} &= -\sqrt{\tilde{\varepsilon}/\beta_1}\left(\sin\psi + \alpha_1 \cos\psi\right). \end{aligned} \tag{25}$$

Substituting these expressions to the equitation describing the longitudinal displacement due to betatron motion, $M_{l_{51}} x_1 + M_{l_{52}} \theta_{x_1}$, and performing simple transformations one obtains the dimensionless amplitude due to betatron motion:

$$a_x = k\sqrt{\tilde{\varepsilon}\left(\beta_1 {M_{l_{51}}}^2 - 2\alpha_1 M_{l_{51}} M_{l_{52}} + \left(1+\alpha_1^2\right){M_{l_{52}}}^2/\beta_1\right)} \ . \tag{26}$$

Averaging momentum kicks over betatron and synchrotron oscillations one obtains the fudge factors for the transverse and longitudinal damping rates:

$$\begin{aligned} &\begin{bmatrix} \lambda_1(a_x,a_p)/\lambda_1 \\ \lambda_2(a_x,a_p)/\lambda_2 \end{bmatrix} \equiv \begin{bmatrix} F_1(a_x,a_p) \\ F_2(a_x,a_p) \end{bmatrix} \\ &= \begin{bmatrix} 2/\left(a_x\cos\psi_c\right) \\ 2/a_p \end{bmatrix} \oint\!\!\oint \sin\left(a_x \sin\left(\psi_x+\psi_c\right) + a_p \sin\psi_p\right) \begin{bmatrix} \sin\psi_x \\ \sin\psi_p \end{bmatrix} \frac{d\psi_x}{2\pi}\frac{d\psi_p}{2\pi} \ , \end{aligned} \tag{27}$$

where $\psi_c$ is the phase shift of the transverse cooling force. Computation of the integrals yields:

$$\begin{bmatrix} F_1(a_x,a_p) \\ F_2(a_x,a_p) \end{bmatrix} = 2\begin{bmatrix} J_0(a_p)J_1(a_x)/a_x \\ J_0(a_x)J_1(a_p)/a_p \end{bmatrix} \ , \tag{28}$$

---

[2] The Courant-Snyder invariant is defined as following: $\tilde{\varepsilon} = x^2/\beta + 2\alpha x\theta + \left(1+\alpha^2\right)\theta^2/\beta$.

where $J_0(x)$ and $J_1(x)$ are the Bessel functions. One can see that the damping rates oscillate with growth of amplitudes. For a given degree of freedom the damping rate changes the sign at its own amplitude equal to $\mu_{11}\approx 3.832$ and at the amplitude of $\mu_{01}\approx 2.405$ for other degree of freedom. Taking into account that the both cooling rates have to be positive for all amplitudes one obtains the stability condition, $a_{x,p} \le \mu_{01} \approx 2.405$. That yields the stability boundaries for the emittance and the momentum spread:

$$\varepsilon_{\max} = \frac{{\mu_{01}}^2}{k^2\left(\beta_p {M_{1_{51}}}^2 - 2\alpha_p M_{1_{51}} M_{1_{52}} + \gamma_p {M_{1_{52}}}^2\right)} \ , \tag{29}$$

$$\left(\frac{\Delta p}{p}\right)_{\max} = \frac{\mu_{01}}{kS_{12}} \ . \tag{30}$$

For further analysis we introduce the relative cooling ranges as ratios of cooling area boundaries $(\Delta p/p)_{\max}$ and $\varepsilon_{max}$ to the rms values of momentum spread, $\sigma_p$, and horizontal emittance, $\varepsilon$. That yields:

$$n_{\sigma s} = (\Delta p / p)_{max} / \sigma_p \ , \quad n_{\sigma x} = \sqrt{\varepsilon_{\max} / \varepsilon} \ . \tag{31}$$

As one can see the transverse cooling range does not depend on the dispersion in the pickup undulator but depends on the beta-function in there. Beam cooling in a collider requires $n_{\sigma x}, n_{\sigma s} \ge 4$.

## 5. Beam Optics and its Limitations

The analysis of possible optics arrangements in the cooling area yielded that the layout presented in Figure 1 is not only the most straightforward but also represents a reliable and effective choice. The cooling chicane consists of four dipoles with parallel edges, which in the absence of other focusing elements does not produce focusing in the horizontal plane resulting in that $M_{1_{56}} = S_{12}$. As one can see from Eq. (18) transverse cooling requires $M_{1_{56}}$ and $S_{12}$ being different. It is achieved by placing a defocusing quad in the chicane center.

To make a simple estimate showing interdependency of cooling parameters we leave only leading terms in the thin lens approximation assuming also that the bends have zero length and do not produce horizontal focusing. That yields:

$$\begin{aligned} &M_{1_{56}} \approx 2\Delta s \ , \quad S_{12} \approx 2\Delta s - \Phi D^* h \ , \\ &\lambda_x / \lambda_s \approx \Phi D^* h / \left(2\Delta s - \Phi D^* h\right). \end{aligned} \tag{32}$$

Here $\Delta s$ and $h$ are the path lengthening and the trajectory offset in the chicane, $\Phi=1/F$ is the defocusing strength of the quad located in the chicane center, and $D^*$ is the dispersion in there. Similarly, using Eq. (31) one obtains estimates for the cooling ranges:

$$n_{\sigma s} \approx \frac{\mu_{01}}{\left(2\Delta s - \Phi D^* h\right) k\sigma_p},$$
$$n_{\sigma x} \approx \frac{\mu_{01}}{2kh\Phi\sqrt{\varepsilon\beta^*}}, \tag{33}$$

where $\beta^*$ is the beta-function in the chicane center. Above we assumed that the optics is symmetric relative to the chicane center, *i.e.* $dD/ds$=0 and $d\beta/ds$=0 in the chicane center. Such choice minimizes the maximal dispersion and beta-function in the cooling area.

**Table 1: Tentative beam optics parameters for the Fermilab OSC test and the LHC**

| | Fermilab OSC test | OSC for the LHC |
|---|---|---|
| Rms momentum spread, $\sigma_p$ | $1.2\cdot10^{-4}$ | $10^{-4}$ |
| Rms emittance, $\varepsilon$, nm | 4.4 | 0.5 |
| Delay in the cooling chicane, $\Delta s$, mm | 2 | 2 |
| Cooling range, $n_{\sigma x}, n_{\sigma s}$ | 3 | 4 |
| Required wave length, μm | 1.8 | 2.1 |
| Dispersion invariant in the chicane center, $A^*$, m | 1.3 | 0.35 |

As one can see from Eq. (32) the parameter $\Phi D^* h$ determines the ratio of cooling rates. Assuming equal damping rates one obtains, $\Delta s = \Phi D^* h$, and, consequently, the cooling ranges are:

$$n_{\sigma s} \approx \frac{\mu_{01}}{k\sigma_p \Delta s},$$
$$n_{\sigma x} \approx \frac{\mu_{01}}{2k\Delta s}\sqrt{\frac{D^{*2}}{\varepsilon\beta^*}} \equiv \frac{\mu_{01}}{2k\Delta s}\sqrt{\frac{A^*}{\varepsilon}}, \tag{34}$$

where $A^*=D^{*2}/\beta^*$ is the dispersion invariant[3] in the chicane center. Its value is conserved in a straight line where bending magnets are absent. As one can see from the above equations the cooling dynamics is determined by a handful of parameters: the initial rms momentum spread and emittance ($\sigma_p$,$\varepsilon$), the wave number of optical amplifier ($k$), the dispersion invariant ($A^*$) and the path length delay ($\Delta s$). The value of $\Delta s$ is determined by signal delay in optical amplifier and normally should be in the range of few mm. Further we will assume $\Delta s$=2 mm – the value expected for the OSC test in Fermilab [12]. Table 1 presents tentative beam optics parameters for the Fermilab OSC test and the LHC operating at 4 TeV. Note that if parameters presented for the Fermilab OSC test represent the actual proposal; the LHC parameters are presented as an

[3] The dispersion invariant is defined as follows: $A_x = D_x^2\left(1+\alpha_x^2\right)/\beta_x + 2\alpha_x D_x' D_x + \beta_x D_x'^2$ . The derivatives of beta-functions and dispersion are equal to zero in the chicane center. That yields: $A^* = D_x^2/\beta_x$.

example only. Note also that one can significantly affect the optics parameters by changing the distribution of cooling rates. In particular, an increase of horizontal damping can allow a reduction of the optical amplifier wavelength, but at the same time it makes more difficult to handle an increase of beta-function in the cooling area required to keep sufficiently large value for the horizontal cooling range.

Large value of the dispersion invariant required for OSC leads to a collider type optics, *i.e.* optics with small value of the beta-function in the chicane center so that the large value of the invariant could be achieved with manageable value of dispersion. Figure 3 presents beta-functions and dispersion in the cooling area for the Fermilab OSC test. Figure 4 shows corresponding dispersion invariant. The equilibrium horizontal emittance is mainly excited by synchrotron radiation and its contribution to diffusion is proportional to the average value of dispersion invariant in dipoles. Therefore the strength of quadrupoles in the chicane vicinity was adjusted so that to reduce the invariant as fast as possible outside of cooling area and, thus, to minimize the equilibrium horizontal emittance. As one can see the value of the invariant is significantly larger than the value presented in Table 1. It allowed significant increase of cooling ranges. It has been required for an improvement of beam lifetime which is mainly determined by particle scattering on atoms of residual gas. The choice of optics supports: $n_{cx} = 9.2$, $n_{cs} = 5.6$, $\lambda_x/\lambda_s = 2.5$. Figure 5 presents dependences for $M_{1_{56}}$ and $S_{12}$ on the beam travel from pickup to kicker. One can see that $S_{12}$ has large variations of its value on the beam travel through the chicane. These variations are excited by large dispersion in the chicane. In the absence of focusing $S_{12}$ and $M_{1_{56}}$ would be equal at the chicane end. Non-zero focusing makes them different. Large $S_{12}$ variations make resulting $S_{12}$ being quite sensitive to optics errors. There is even higher sensitivity of sample lengthening to optics errors in the case of betatron motion. Figure 6 presents sample lengthening due to betatron motion. One can see that the final lengthening is about 300 times smaller than its peak value located between chicane dipoles.

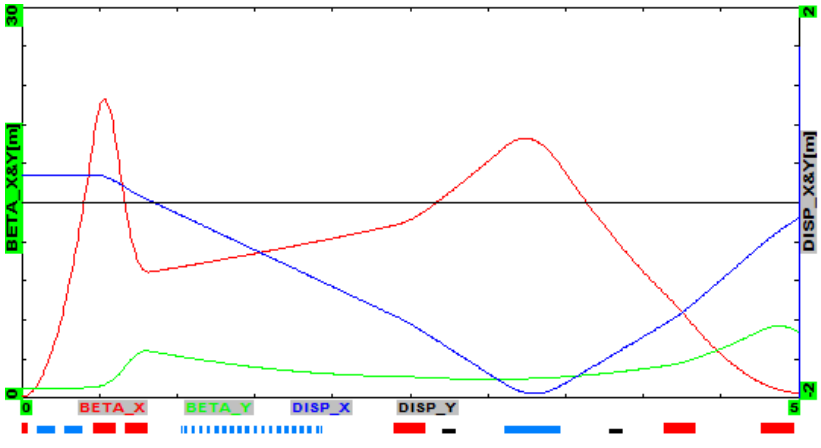


Figure 3: Beta-functions ($\beta_x$ – red, $\beta_y$ – green) and dispersion (dark blue) for half of cooling area of the Fermilab OSC test. Chicane center is located at $s = 0$; red squares at the bottom mark positions of quadrupoles, the blue squares – dipoles and undulator.

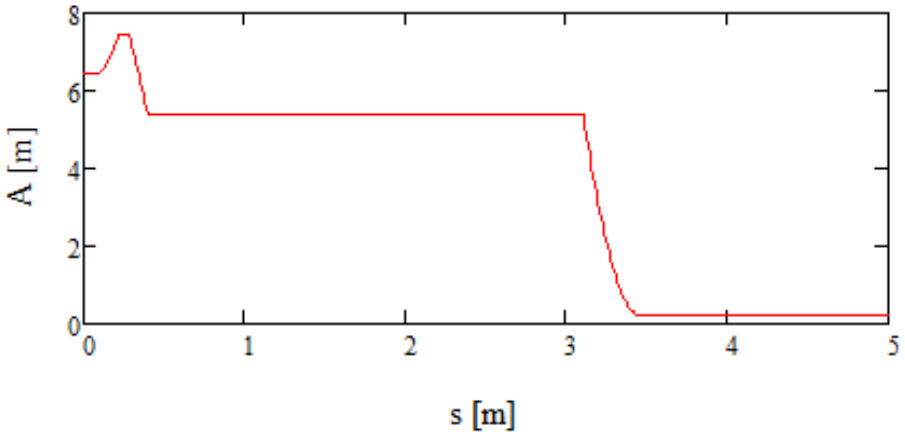


Figure 4: The dispersion invariant, $A_x$, for half of cooling area of the Fermilab OSC test.

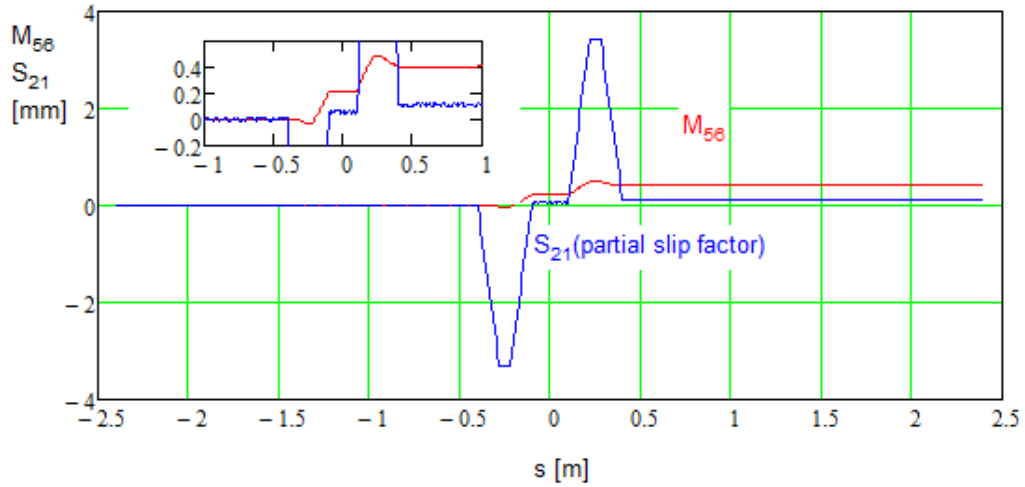


Figure 5: Dependence of $M_{56}$ and $S_{12}$ in the cooling area of the Fermilab OSC test; $s = 0$ corresponds to the chicane center.

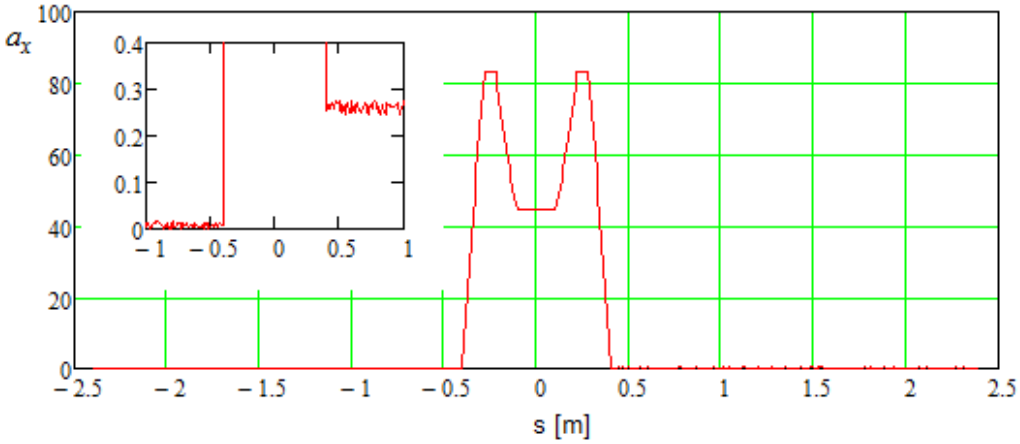


Figure 6: Dimensionless rms sample lengthening due to betatron motion, $a_p$, in the cooling area of the Fermilab OSC test; $s = 0$ corresponds to the chicane center.

Another important limitation on the beam optics is associated with the higher order contributions to the sample lengthening coming from the betatron and synchrotron motions. The major contribution comes from particle angle, $\theta(s)$, which introduce the relative delay $\Delta s/s$ equal to $\theta(s)^2/2$. To obtain the particle angle on the way from pickup to kicker we differentiate its horizontal position $x(s)=\sqrt{\varepsilon\beta(s)}\cos\left(\mu(s)-\mu_0\right)$ over $s$. An integration of square of the obtained angle yields the orbit lengthening:

$$\begin{aligned}\Delta s_2 &= \frac{1}{2}\int_{-L_c/2}^{L_c/2}\left(\sqrt{\frac{\varepsilon}{\beta(s)}}\left(\sin\left(\mu(s)-\mu_0\right)+\alpha(s)\cos\left(\mu(s)-\mu_0\right)\right)\right)^2 ds \\ &= \frac{\varepsilon}{2}\int_{-\mu_c/2}^{\mu_c/2}\left(\sin\left(\mu-\mu_0\right)+\alpha(\mu)\cos\left(\mu-\mu_0\right)\right)^2 d\mu\,.\end{aligned} \tag{35}$$

Here $\mu_0$ is the initial betatron phase, $\mu$ is the betatron phase advance along the particle trajectory, $L_c$ is the total path length from pickup to kicker, and we took into account that $d\mu=ds/\beta$. Assuming that the optics in the cooling area is symmetric relative to the chicane center one can reduce Eq. (35) to the following form:

$$\begin{aligned}\Delta s_2 &= \frac{\varepsilon}{2}\left(I_1 - I_2\cos(2\mu_0)\right), \\ I_1 &= \int_0^{\mu_c/2}\left(1+\alpha^2(\mu)\right)d\mu\,, \\ I_2 &= \int_0^{\mu_c/2}\left(\left(1-\alpha^2(\mu)\right)\cos(2\mu)-2\alpha(\mu)\sin(2\mu)\right)d\mu\,,\end{aligned} \tag{36}$$

where $\mu_0$ is related to the particle betatron phase in the chicane center. The maximum lengthening is achieved for $\mu_0=\pi/2$ and is equal to: $\Delta s=\varepsilon\left(I_1+I_2\right)/2$.

Numeric averaging of cooling force with the second order lengthening taken into account shows that to avoid shrinking of cooling boundary the second order contribution at the cooling boundary has to be less or about half of the first order contribution (see Eq. (26)). That yields the requirement on an acceptable value of the second order contribution computed at the boundary of cooling range (defined by Eq. (29)): $k\Delta s_2 \le 1.5$.

Figure 7 presents integrals $I_1$ and $I_2$ as functions of path length for the Fermilab OSC test. One can see that the values of integrals are significantly larger for the horizontal plane. It is related to the small beta-function in the chicane center which yields large particle angles in the area between focusing doublets, $\theta=\sqrt{\varepsilon/\beta^*}$. In this case the total lengthening can be estimated by simple formula: $\Delta s \approx L_q\varepsilon/2\beta^*$, where $L_q$ is the distance between quadrupole doublets. For the Fermilab OSC test the non-linear path lengthening due to vertical betatron motion is 0.017 μm at 1σ and does not represent a problem. However its value for the horizontal plane of 0.25 μm at 1σ destroys cooling for betatron amplitudes above 1.5σ and therefore has to be compensated.

The compensation is achieved by placing a sextupole in between dipoles of each chicane leg. It decreases the sample lengthening by more than an order of magnitude so that the contribution for the horizontal plane is smaller than for the vertical one. The sextupoles are located at the betatron phase advance close to 180 deg. It significantly decreases the driving terms of sextupole related resonances. However the compensation is not perfect and an additional suppression by ring sextupoles is required. They also have to compensate undesired chromaticity introduced by the chicane sextupoles.

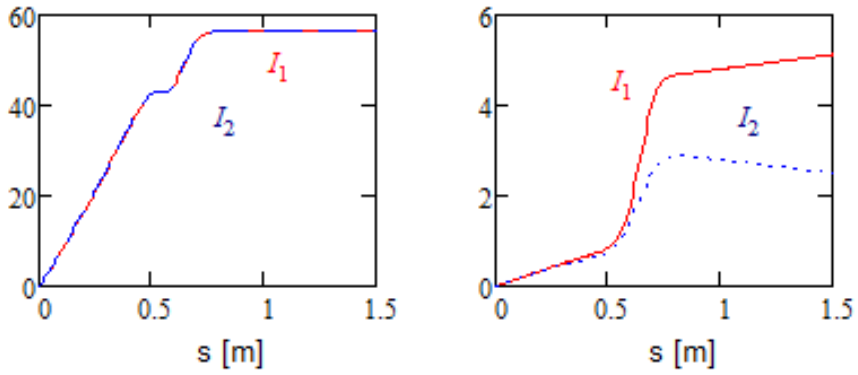


Figure 7: Integrals $I_1$ (red) and $I_2$ (blue) of Eq. (36) in the cooling area of the Fermilab OSC test; horizontal plane – left, vertical plane – right.

## 6. Damping Rates

To compute the OSC damping rates we need to find a longitudinal kick which a particle receives in the kicker undulator from its own radiation radiated in the pickup undulator and then amplified and focused to the kicker undulator. We split this problem into the following steps: finding electric field of the radiation on the focusing lens surface, computing the electric field in the kicker undulator by integration of the field distribution on the lens, and, finally, finding the longitudinal kick in the kicker undulator. We assume that the distances from the pickup center to the lens and from the lens to the kicker center are equal and are much larger than the pickup and kicker lengths; so large that the depth of field would not result in a deterioration of the interaction. Applicability of such requirement will be discussed later. We also assume that the pickup and kicker undulators are flat, have the same length and the same number of periods.

The e.-m. radiation coming out from the pick-up undulator is determined by the Liénard-Wiechert formula [14]:

$$\mathbf{E}(\mathbf{r},t)=\frac{e}{c^2}\frac{(\mathbf{R}-\boldsymbol{\beta}R)(\mathbf{a}\cdot\mathbf{R})-\mathbf{a}(R-(\boldsymbol{\beta}\cdot\mathbf{R}))}{(R-(\boldsymbol{\beta}\cdot\mathbf{R}))^3},\quad \mathbf{a}=\frac{d\mathbf{v}}{dt},\quad \mathbf{R}=\mathbf{r}-\mathbf{r}'\quad . \tag{37}$$

Here $e$ is the particle charge, $\boldsymbol{\beta}=\mathbf{v}/c$ is the dimensionless particle velocity, $\mathbf{R}$ is the vector from point of the radiation, $\mathbf{r}'$, to the point of observation, $\mathbf{r}$, and all values are taken at the retarded time $t'=t-R/c$. Let the coordinates of a particle moving in a flat undulator to depend on time as following:

$$\mathrm{v}_x = c\theta_e \sin\tau', \qquad \mathrm{v}_y = 0,$$
$$\mathrm{v}_z = c\left(1 - \frac{1}{2\gamma^2} - \frac{\theta_e^2}{2}\sin^2\tau'\right), \quad \tau' = \omega_u t' + \psi, \tag{38}$$

where $\omega_u$ is the frequency of particle motion in the undulator, and $\theta_e$ is the amplitude of particle angle oscillations. Substituting velocities of Eq. (38) to Eq. (37) and simplifying the obtained equation one obtains the horizontal component of electric field in the far zone:

$$E_x(r,t) = 4e\omega_u\gamma^4\theta_e\cos\tau' \frac{1+\gamma^2\left(\theta^2\left(1-2\cos^2\phi\right) - 2\theta\theta_e\sin\tau'\cos\phi - \theta_e^2\sin^2\tau'\right)}{cR\left(1+\gamma^2\left(\theta^2 + 2\theta\theta_e\sin\tau'\cos\phi + \theta_e^2\sin^2\tau'\right)\right)^3}, \tag{39}$$

where $\theta$ and $\phi$ are the angles in the polar coordinate frame for the vector **R**, and we took into account that $a_x = c\theta_e\omega_u$ . The vertical and longitudinal components of the electric field are averaged out at the focus and therefore can be safely omitted from further consideration.

Only the first harmonic of the radiation interacts resonantly with the particle in the kicker undulator. Therefore we keep only the first harmonic of radiation in further calculations:

$$E_\omega(r) = \frac{\omega(\theta)}{\pi}\int_0^{2\pi/\omega(\theta)} E_x(r,t)\mathrm{e}^{-i\omega t}\,dt, \qquad \omega(\theta) = 2\gamma^2\omega_u / \left(1+\gamma^2\left(\theta^2 + \theta_e^2/2\right)\right). \tag{40}$$

Omitting higher harmonics is also justified by the fact that their radiation is usually absorbed in the lens(es) focusing radiation from the pickup to the kicker and is not amplified by optical amplifier (if present).

To find the electric field in the kicker undulator, where the radiation is focused, we use the Kirchhoff formula:

$$E(r'') = \frac{1}{2\pi ic}\int_S \frac{\omega(\theta)E_\omega(r)}{|r''-r|}\mathrm{e}^{i\omega(\theta)|r''-r|/c}\,ds\ . \tag{41}$$

Here $r''$ is the coordinate in the observation point in the kicker undulator, the integration is performed over the lens surface *S*, and the electric field there is described by Eqs. (39) and (40). The focal length of the lens is equal to *R*/2. It results in that an increase of delay time related to path lengthening, $2\left(R\theta^2/2\right)$, is compensated in the lens. It makes all waves arriving to the focus point having the same phase, and, consequently, the exponent in Eq. (41) accounting for these delays is reduced to a complex constant which will be omitted in further calculations. Note that although the frequency of radiation coming out from radiation point depends on $\theta$ this dependence disappears in the kicker undulator (in the image plane) due to interference of the waves coming from different directions.

The above equations can be significantly simplified in the case of small undulator parameter, $K=\gamma\theta_e<<1$. Then Eq. (39) can be simplified yielding the wave amplitude on the lens surface:

$$E_x = \frac{4e\gamma^4\omega_u\theta_e}{cR}\,\frac{1+(\gamma\theta)^2(1-2\cos\phi)}{\left(1+(\gamma\theta)^2\right)^3}, \tag{42}$$

The dependence of frequency on $\theta_e$ can be neglected and an integration in Eq. (41) results in the amplitude of electric field in the kicker undulator:

$$E_x = \frac{4e\gamma^4\omega_u{}^2\theta_e}{3c^2}\,f_L(\gamma\theta_{\rm m}), \quad f_L(x) = 1-\frac{1}{\left(1+x^2\right)^3}\ . \tag{43}$$

Here $\theta_{\rm m}$ is the angle subtending the lens from the pickup undulator and we assume a round lens. Averaging the energy transfer ($d$E/dt=$e$E$_x$v$_x$) over oscillations in the kicker undulator we finally obtain the amplitude of the energy change in the kicker undulator in the absence of optical amplification:

$$\Delta{\rm E} = \frac{2e^4B_0{}^2\gamma^2}{3m^2c^4}L_u\ f_L\left(\gamma\theta_{\rm m}\right)\ . \tag{44}$$

Here $B_0$ is the peak magnetic field in the undulator, $L_u$ is its total length, and $m$ is the particle mass. We also took into account that $\theta_e = eB_0/\left(mc\gamma\omega_u\right)$.

Note that in the absence of optical amplification and $\gamma\theta_{\max} >> 1$ the amplitude of energy loss is equal to the total energy loss in both undulators: $\Delta{\rm E}_{tot} = 2e^4B_0{}^2\gamma^2L_u/\left(3m^2c^4\right)$. The interference of radiation of two undulators results in the energy loss being modulated with the path length difference on the travel from pickup to kicker: $\Delta{\rm E}(\Delta s) = -\Delta{\rm E}_{tot}\left(1+\cos(k\Delta s)\right)$. For longitudinal motion we can rewrite it as:

$$\Delta{\rm E}(\Delta p) = -\Delta{\rm E}_{tot}\left(1+\cos\left(kS_{12}\frac{\Delta p}{p}\right)\right)\ . \tag{45}$$

Taking into account that the damping decrement is proportional to $d\Delta{\rm E}/dp$ one obtains that the interference of radiation from two undulators amplifies the damping rate due to their synchrotron radiation by the ratio of beam energy to it's the cooling range, $p/n_{\sigma p}\sigma_p$. The same statement is justified for the betatron motion. Note that an average energy loss presented in Eq. (45) is compensated by an RF system and does not effect on the cooling dynamics.

The cooling rates are determined by Eqs. (18) and (20) where parameters $k$ and $\kappa$ introduced in Eq. (2) are equal to:

$$\begin{aligned} k &= \frac{2\gamma^2\omega_u}{c}, \\ \kappa &= \frac{2e^4B_0{}^2\gamma}{3m^3c^5}L_u\ K_a f_L\left(\gamma\theta_{\rm m}\right). \end{aligned} \tag{46}$$

Here we added an effect of e.-m. wave amplification in an optical amplifier with gain $K_a$ (in

amplitude). We also assume that the bandwidth of optical amplifier is large enough so that the spectrum widening due to finite number of undulator periods $2\gamma^2\omega_u / n_w$ and the angular spread of radiation $2\gamma^4\omega_u\theta_{\max}$ would be inside the amplifier bandwidth. Here $n_w$ is the number of undulator periods. Otherwise one needs to average the cooling force within amplifier bandwidth. Note also that for large amplitude oscillations the fudge factors introduced in Eqs. (27) and (28) have to be taken into account.

In the general case of arbitrary undulator parameter the amplitude of electric field in the kicker undulator can be expressed in the following form:

$$E_x = \frac{4e\omega_u{}^2\gamma^4\theta_e}{3c^2} F_h\left(\gamma\theta_e, \gamma\theta_m\right) , \tag{47}$$

where

$$\begin{aligned} F_h\left(\Theta_e,\Theta_m\right) &= \frac{3}{\pi^2}\int_0^{\Theta_m} d\Theta \int_0^{2\pi} d\phi \int_0^{2\pi} d\tau \frac{\Theta F_c\left(\Theta,\Theta_e,\tau,\phi\right)}{1+\Theta^2+\frac{\Theta_e{}^2}{2}} \frac{1+\Theta^2\left(1-2\cos^2\phi\right)-2\Theta\Theta_e\cos\phi\sin\tau-\Theta_e{}^2\sin^2\tau}{\left(1+\Theta^2+2\Theta\Theta_e\cos\phi\sin\tau+\Theta_e{}^2\sin^2\tau\right)^3}, \\ F_c\left(\Theta,\Theta_e,\tau,\phi\right) &= \left(1+\frac{4\Theta\Theta_e\cos\phi\sin\tau-\Theta_e{}^2\cos\left(2\tau\right)}{2\left(1+\Theta^2+\frac{\Theta_e{}^2}{2}\right)}\right)\exp\left(-i\tau+i\frac{\Theta_e{}^2\sin\left(2\tau\right)+8\Theta\Theta_e\cos\phi\cos\tau}{4\left(1+\Theta^2+\frac{\Theta_e{}^2}{2}\right)}\right)\cos\tau . \end{aligned} \tag{48}$$

For the large acceptance lens, $\theta_m \geq \theta_e + 3/\gamma$ the function $F_h\left(\Theta_e,\theta_m\right)$ computed with numerical integration can be interpolated by the following equation:

$$F_h\left(K,\infty\right) \approx \frac{1}{1+1.07K^2+0.11K^2+0.36K^4}, \quad 0 \leq K \leq 4 . \tag{49}$$

Integrating the force along the kicker length one obtains the longitudinal kick amplitude in a flat undulator:

$$\Delta \mathrm{E} = \frac{2\pi}{3}\alpha_F n_w \hbar\omega_0 K^2\left(1+\frac{K^2}{2}\right)F_h\left(K,\gamma\theta_m\right)F_u\left(\kappa_u\right), \quad \begin{aligned} F_u\left(\kappa_u\right) &= \mathrm{J}_0\left(\kappa_u\right)-\mathrm{J}_1\left(\kappa_u\right), \\ \kappa_u &= K^2/\left(4\left(1+K^2/2\right)\right). \end{aligned} \tag{50}$$

Here $\alpha_F = e^2/\hbar c$ is the fine structure constant, and $\omega_0 = 2\gamma^2\omega_u\left(1+K^2/2\right)$ is the base frequency of the radiation. For small $K$ this equation coincides with Eq. (44). Figure 8 presents a dependence of dimensionless kick, $F_t(K,\gamma\theta_m) = K^2\left(1+K^2/2\right)F_h\left(K,\gamma\theta_m\right)F_u\left(\kappa_u\right)$, on the undulator parameter for different values of $\gamma\theta_m$. The same as above we imply here that the optical amplifier gain is equal to one and its bandwidth is larger than the bandwidth of the first harmonic radiation coming from the pickup undulator. Otherwise averaging over the bandwidth is additionally required.

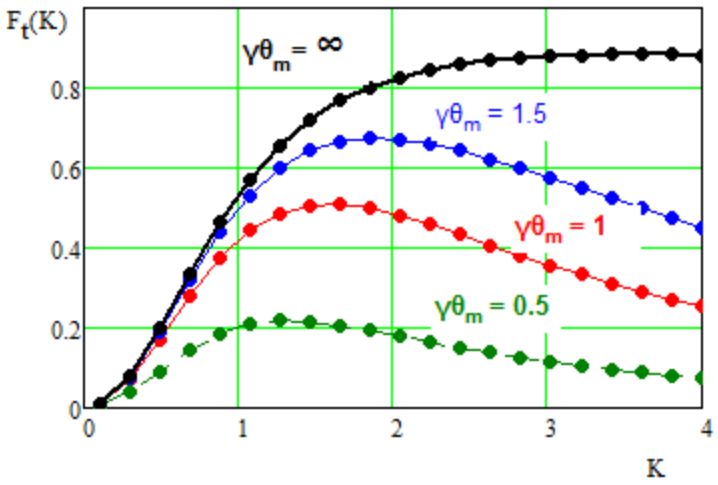


Figure 8: Dependence of dimensionless longitudinal kick on the undulator parameter.

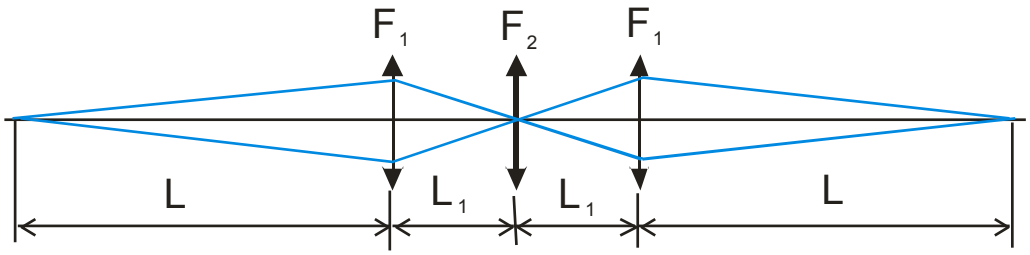


Figure 9: Light optics layout for passive cooling.

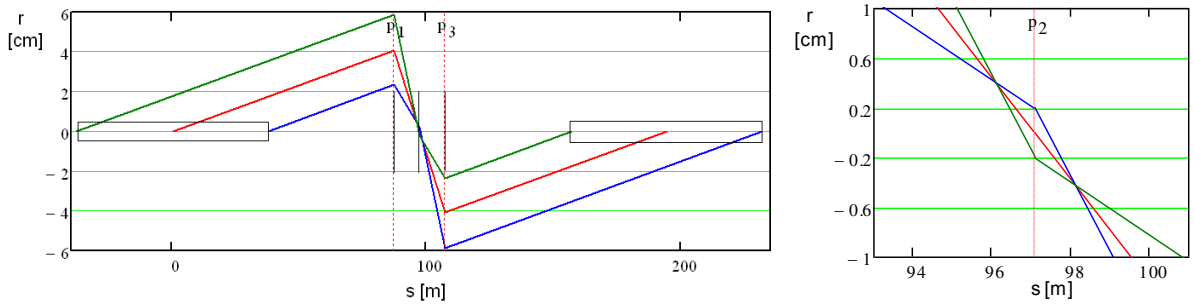


Figure 10: Trajectories of rays radiated at the beginning, in the middle and at the end of pickup undulator. Right pain shows details near the center of the system. Vertical lines show positions of the lenses.

## 7. Light optics

Above we assumed that the radiation emitted by a particle in the course of its motion in the pickup is focused to the location of the same particle in the kicker (when the particle arrives to it) in the course of particle entire motion in the kicker. It is automatically achieved for the lens located at the infinity (*i.e.* if the distance to the lens is much larger than the length of undulator) – the condition which is impossible to achieve in practice. A practical solution can be obtained with lens telescope which has the transfer matrix $\mathbf{M}_T$ from the center of pickup to the center of kicker equal to $\pm\mathbf{I}$, where $\mathbf{I}$ is the identity matrix. In this case the transfer matrix between

emitting and receiving points is $\mathbf{O}(l)\mathbf{M}_T\,\mathbf{O}(-l) = \pm\mathbf{I}$, *i.e.* coincides with the matrix for the system where the lens is located at infinity. Here $\mathbf{O}(l)$ is the transfer matrix of a drift with length $l$. The simplest telescope requires 3 lenses. An example is presented in Figure 9. For symmetrically located lenses their focusing distances are:

$$F_1 = \frac{LL_1}{L+L_1}, \quad F_2 = \frac{L_1^2}{2\left(L+L_1\right)} \quad . \tag{51}$$

Here $F_1$ is the focal distance for two outer lenses, and $F_2$ is the focal distance for the central lens. Figure 10 presents an example of ray propagation through such focusing system. As one can see the light focus is propagated together with particle displacement in the kicker undulator.

## Conclusions

The optical stochastic cooling can support the cooling rates orders of magnitude larger than have been achieved with the micro-wave stochastic cooling. Its experimental study is required before it can be used in practical application for high intensity storage rings and hadron colliders. Such applications will require a new generation of optical amplifiers with the following requirements: (1) small signal delay (less than few mm), (2) large gain (more than ~20-30 Db), duration of single pulse amplification sufficient to cover a bunch of cooled particles (0.1-1 ns), and (3) sufficiently large power (10 – 100 W). Fermilab plans to do the OSC tests with 100 MeV electrons in the IOTA ring [12] within next few years. Choice of small energy electrons greatly simplifies the experiment and reduces its cost.

**Acknowledgements:** *The author would like to express sincere gratitude to Max Zolotorev for initiating this work, for multiyear collaboration and many contributions without which this work would not be possible.*

## References

[1] S. Van der Meer, "Stochastic damping of betatron oscillations", internal report CERN/ISR PO/72/31 (1972).
[2] R. Billinge and M. C. Crowley-Milling, "The CERN proton-antiproton colliding beam facilities", IEEE Transactions on Nuclear Science, Vol. NS-26, No. 3, June 1979.
[3] J. Bisognano and C. Leemann, "Stochastic Cooling" in 1981 Summer School on High Energy Particle Accelerators, AIP Conf. Proceedings 87, Melville, NY, 1982, pp. 584-655.
[4] V. Lebedev and V. Shiltsev (Eds.), "Accelerator Physics at the Tevatron Collider", Springer, 2014.
[5] M. Blaskiewicz, J. M. Brennan, F. Severino, "Stochastic Cooling of High-Energy Bunched Beams", Proceedings of PAC07, Albuquerque, New Mexico, USA.
[6] M. S. Zolotorev and A. A Zholents, "Transit-time method of optical stochastic cooling", Phys. Rev. E, 50, 4, p. 3087 (1994).
[7] A. Zholents and M. Zolotorev, "An amplifier for optical stochastic cooling", p. 1804, PAC'97 (1997).
[8] V. Lebedev, "Optical Stochastic Cooing in Tevatron", Proceedings of HB2010, Morschach, Switzerland, 2010.
[9] M. Babzien, et.al, "Optical stochastic cooling for RHIC using optical parametric amplification", PRST-AB, 7, 012801 (2004).
[10] W. Franklin, et. al., "Optical Stochastic Cooling Experiment at the MIT-Bates South Hall Ring", p. 117, COOL-2007 (2007)
[11] V. Lebedev, "Test of Optical Stochastic Cooling in Fermilab", Proceedings of HB2012, Beijing, China.

[12] V. Lebedev, “Test of Optical Stochastic Cooling in the IOTA Ring”, Proceedings of PAC2013, Pasadena, CA USA.
[13] A. Burov and V. Lebedev, “Coupling and its Effects on Beam Dynamics”, Proceedings of Hadron Beam 2008, Nashville, Tennessee, USA.
[14] L. D. Landau, “Classical theory of fields”, Nauka (1973).